

Safe Autonomous Environmental Contact for Soft Robots using Control Barrier Functions

Akua K. Dickson^{1*}, Juan C. Pacheco Garcia^{2*}, Meredith L. Anderson², Ran Jing², Sarah Alizadeh-Shabdiz², Audrey X. Wang², Charles DeLorey³, Zach J. Patterson⁴, Andrew P. Sabelhaus^{1,2†}

Abstract—Robots built from soft materials will inherently apply lower environmental forces than their rigid counterparts, and therefore may be more suitable in sensitive settings with unintended contact. However, these robots’ applied forces result from both their design and their control system in closed-loop, and therefore, ensuring bounds on these forces requires controller synthesis for safety as well. This article introduces the first feedback controller for a soft manipulator that formally meets a safety specification with respect to environmental contact. In our proof-of-concept setting, the robot’s environment has known geometry and is deformable with a known elastic modulus. Our approach maps a bound on applied forces to a safe set of positions of the robot’s tip via predicted deformations of the environment. Then, a quadratic program with Control Barrier Functions in its constraints is used to supervise a nominal feedback signal, verifiably maintaining the robot’s tip within this safe set. Hardware experiments on a multi-segment soft pneumatic robot demonstrate that the proposed framework successfully constrains its environmental contact forces. This framework represents a fundamental shift in perspective on control and safety for soft robots, defining and implementing a formally verifiable logic specification on their pose and contact forces.

I. INTRODUCTION

Robots built from soft and deformable materials are often claimed to be inherently ‘safe’ or ‘safer’ than their rigid counterparts [1], [2], [3], [4], [5]. The soft robotics community justifies this claim via the robots’ compliance to their environments, deforming upon contact, which applies lower external forces from the robot’s body [6]. This understanding aligns well with many intended purposes of soft robots, such as medical operations [7] or other intimate human-robot contact [8], [9].

However, little prior work in soft robotics has defined ‘safety’ as a technical term, which would be required for an engineering analysis – when and how are soft robots safer,

This work was in part supported by the U.S. National Science Foundation under Award No. 2340111, 2209783, and a Graduate Research Fellowship.

¹A.K. Dickson and A.P. Sabelhaus are with the Division of Systems Engineering, Boston University, Boston MA, USA. {akuaad, asabelha}@bu.edu

²M.L. Anderson, J.C. Pacheco Garcia, R. Jing, S. Alizadeh-Shabdiz, A.X. Wang, and A.P. Sabelhaus are with the Department of Mechanical Engineering, Boston University, Boston MA, USA. {merland, jcp29, rjing, sar3, axwang}@bu.edu

³C. DeLorey is with the School of Electronic and Electrical Engineering, University of Leeds, Leeds, UK. (elchd@leeds.ac.uk)

⁴Z. Patterson is with the Department of Mechanical and Aerospace Engineering, Case Western Reserve University, Cleveland, OH, USA. (zpatt@case.edu)

* Equal Contribution.

† Corresponding author.

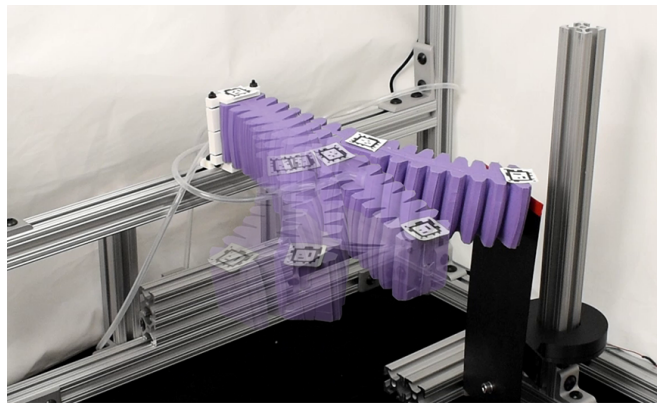


Fig. 1. This article proposes a feedback control method for a soft robot manipulator (purple) to meet a formal safety specification on its environmental contact forces. We assume the environment (black flexible plate) deforms and is known, and so safe forces map to safe poses. Control barrier functions ensure the robot remains within the set of safe poses.

mathematically? The most promising definition for ‘safety’ comes from the control systems community as constraint satisfaction or a logic specification. A control designer describes a range of acceptable values of some states of a dynamical system, possibly varying or interleaved over time, and if the system maintains these values for all time then it is *safe*: the set is invariant under the dynamics [10]. The invariance perspective (equivalently called reachability [11], [12] or persistent feasibility [13]) is a powerful tool that has revolutionized legged robot locomotion [14], aerial vehicles [15], and rigid human-robot interaction [16], [17].

Attempts at applying invariance to soft robots have shown that, in contrast to common claims, *soft robots do not satisfy safety conditions automatically*. For example, soft actuators can fail by exceeding their operational limits [18], [19], and soft robots can collide with themselves [20]. This is intuitive upon further consideration: one may always actuate a soft robot too quickly, too strongly, to exceed some condition. Prior work has designed invariance-based feedback controllers to ensure safety is maintained in these specialized settings.

This manuscript proposes that closed-loop control is a necessary condition for safety verification of a soft robot’s motion writ large, and in particular, its environmental contact forces: the reason for being of soft robots. We adapt the approach of control barrier functions (CBFs) [21], [22], [23] to meet a set invariance condition on the end effector poses of a soft manipulator. Then, we take the proof-of-concept situation where the robot exists in a deformable environment (Fig. 1), such as when contacting tissue in a

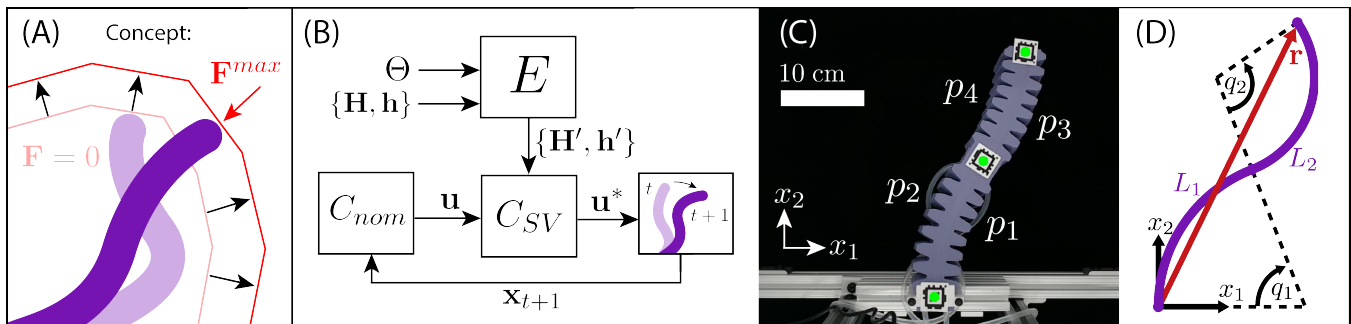


Fig. 2. Our setup (A) maps a soft robot manipulator’s end effector force to its pose by assuming the environment deforms, so a maximum force corresponds to a constraint on the robot’s states. Our approach (B) calculates this set as a polytope $\mathbf{H}'\mathbf{r} \leq \mathbf{h}'$ given an undeformed environment surface $\mathbf{H}\mathbf{r} = \mathbf{h}$ and material parameters Θ , where a supervisory controller C_{SV} filters a nominal control signal to maintain the end effector \mathbf{r} in the safe set. Our application and experiment (C) is a planar two-segment pneumatic robot with antagonistic actuation chambers (p_i, p_{i+1}). Our model (D) is the standard constant-curvature parameterization.

patient, and show how a constraint on external forces could be mapped to a state constraint. We demonstrate that a standard formulation of CBF-based control can meet this constraint in both simulation and hardware experiments (Fig. 2), and verify that our controller maintains a positive *safety margin* on force when an open-loop controller does not.

A. Paper Contributions

This article contributes:

- A method for mapping environmental forces to an open-chain manipulator’s state space, with a one-to-one mapping of a set inclusion criterion between them,
- An adaptation of CBF-based control to a soft robot in this setting, with a proof-by-construction of invariance of the robot’s applied forces,
- A validation in both simulation and hardware that shows our method achieves a positive safety margin on a set of safe forces.

To our knowledge, this manuscript establishes the first formal methods approach that meets a force safety specification in autonomous motions of a soft robot manipulator.

II. BACKGROUND AND PRIOR WORK

Significant prior work exists on autonomy and feedback control of soft robots, particularly for manipulation tasks, yet theoretical concerns exist for the most common control goals, and no prior work has provided a formal proof of force constraints. Controllers for soft or continuum robots have typically set the goal of stability, precision, or low-error trajectory tracking in either state space or task space [24], [25], [26], [27], [28], [29]. However, a paradox arises in precision: it has been shown that decreasing the tracking error of a flexible robot using feedback control will increase its stiffness [30]. So by seeking precise motions, these control systems are necessarily stiffening their soft robots, undercutting the narrative about softness. Control goals such as disturbance rejection [31] may even be antithetical to softness, as they prevent a soft robot from complying to its environment. No prior work, to the authors’ knowledge, has resolved this inconsistency – whereas our safety-based controller does not suffer from the same tradeoff.

Similarly, feedback controllers that consider interaction forces on soft robots or soft substrates do not typically provide formal verification (i.e. safety). Impedance control can modulate forces toward a desired setpoint [32], [33] but does not bound them with a safety specification.

Model-free control of soft robots, or methods that involve machine learning, may have good performance on error tracking [34], [35] but without the provable properties of safety-critical control. Learned dynamics [36], [37] or learned feedback controllers [38] notoriously suffer from unpredictable behaviors in situations outside the training data due to their “black box” operation. Finite element methods have yet to consider safety [39], [40], and most real-time methods use dimensionality reduction [39], [41], [40], [42] which can have limitations representing physically-relevant constraints in the learned state space. These same issues extend to robotics in general, where learning with safety typically requires analytical models (not data-driven) to meet a specification in safety-critical regions [11], [43], [44] or bespoke safe checks manually specified by a designer [45].

When using an analytical dynamics model, multiple definitions exist for ‘safety,’ though the control systems community has recently coalesced around set invariance [46] or similar notions of continuous operation [47]. In soft robotics, this could correspond to fault detection [48], which unfortunately does not have the continuous response of barrier function methods [23], [20]. Alternatively, authors have defined ‘safety’ as a comparison of regions of attraction between controllers [49] or input-to-state stability [50], which are not formal safety conditions as the system may still violate a specification on safety-critical signals.

III. FORCE SAFETY IN DEFORMABLE ENVIRONMENTS

To the authors’ knowledge, this is the first work that allows a soft robot to contact its environment assuming there is some limit of safe force application to that environment. We take inspiration from the work of Liu and Althoff [51], which maps the kinematics of a rigid manipulator to force-safe states under deformations, and Dyck et al. [33] which calculates forces per level sets of geometry normal to a contact surface. Our definition of *force safety* is therefore the same as in these manipulation problems:

Definition 1: Force safety. Trajectories of a (soft) robot’s end effector, $\mathbf{r}(t)$, are force-safe if the applied force at that end effector $\mathbf{F}(t)$ remains within a set of acceptable forces \mathcal{F}^{safe} , or equivalently, \mathcal{F}^{safe} is invariant under the system’s dynamics: $\mathbf{F}(0) \in \mathcal{F}^{safe} \Rightarrow \mathbf{F}(t) \in \mathcal{F}^{safe} \forall t$.

In this section, we demonstrate how, under mild assumptions about the environment, our force safety condition also maps to a set constraint on the robot’s kinematics. We provide a calculation to convert the no-contact set constraint to our contact-aware set constraint.

A. Problem Setup

To synthesize a control system that ensures force safety of our soft robot’s end effector, we consider a first proof-of-concept problem setup for a planar robot, while emphasizing the generalizability as well as straightforwardness to relax in future work (for example, to 3D manipulators).

- 1) The set of manipulator tip positions $\mathbf{r} \in \mathbb{R}^2$ with no environmental contact is represented by a polytope with P -many facets, $\mathcal{N} = \{\mathbf{r} | \mathbf{H}\mathbf{r} \leq \mathbf{h}\}$, with $\mathbf{H} \in \mathbb{R}^{P \times 2}$, $\mathbf{h} \in \mathbb{R}^P$ having no redundant edges. In other words, the boundary of this set $\partial\mathcal{N} = \{\mathbf{r} | \mathbf{H}\mathbf{r} = \mathbf{h}\}$ is the environment’s surface.
- 2) Each facet of the polytope, i.e. the line formed by the row $\mathcal{L}_i = \{\mathbf{r} | \mathbf{H}_i\mathbf{r} = h_i\}$, is deformable and deforms only in the normal direction, $\hat{\mathbf{n}}_i \perp \mathcal{L}_i$.
- 3) Upon contact with the manipulator tip at time t , the surface is deflected to the location of the tip $\mathbf{r}(t)$ in space, $\mathcal{L}'_i = \{\mathbf{r} | \mathbf{H}'_i\mathbf{r} = h'_i\}$ where H'_i and h'_i are such that $\mathbf{n}_i = n_i\hat{\mathbf{n}}_i = \|\mathbf{r}(t) - \text{proj}_{\mathcal{L}_i}\mathbf{r}(t)\|$ is the normal distance between \mathcal{L}_i and \mathcal{L}'_i .
- 4) The force-deformation relationship, now only dependent on the distance of the tip to the i -th surface, $n_i \in \mathbb{R}$, is $\mathbf{F}_i(n_i) = \psi_i(n_i)\hat{\mathbf{n}}_i$. We only consider normal forces.
- 5) The scalar force relationship $\psi_i(\cdot) : \mathbb{R} \mapsto \mathbb{R}$ is strictly monotonic for $n_i > 0$ and is $\psi = 0$ for $n \leq 0$, and is therefore invertible.
- 6) The maximum normal force tolerable by each surface is known a-priori, and therefore $\mathcal{F}^{safe} = \{\mathbf{F} | \|\mathbf{F}_i\| \leq F_i^{max} \forall i\}$ with $\mathbf{F} = \sum_i \mathbf{F}_i$.

In addition, our calculations simplify under the assumption of uniform properties of each facet of the environment, chosen in this work primarily for clarity of our exposition:

- 7) $\psi_i(\cdot) = \psi(\cdot)$, $F_i^{max} = F^{max}$, $\forall i = 1 \dots P$

Fig. 3 is helpful in interpreting these geometric quantities.

We emphasize that these assumptions are not inherent limitations of the concept. Rather, they simplify the edge cases of our calculation, such as force safety at the vertices of \mathcal{N} . Extensions to nonuniform environments, nonconvex environments, 3D environments, and environments with shear/friction are discussed in our future work. The assumption of a static environment can be readily relaxed via the methods of Liu and Althoff [51], and more general geometries by the work of Dyck et al. [33]. In any case, these conditions are surprisingly general: for example, \mathcal{N} can be discretized arbitrarily to approximate smoother surfaces, relaxing (1)-(3), and an environment with a positive Poisson ratio and

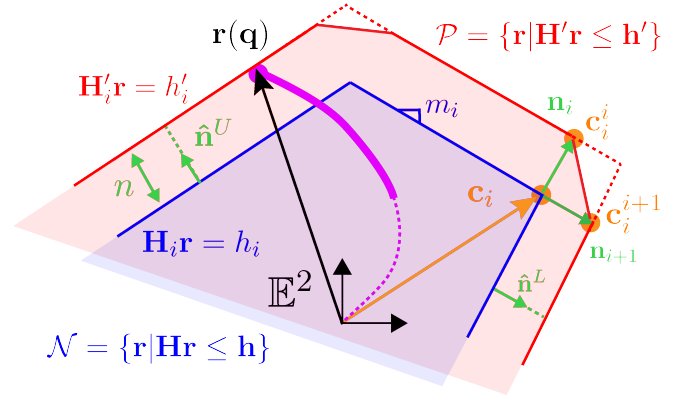


Fig. 3. The deformable environment is represented by a no-contact (free space) set, \mathcal{N} . We assume each face deforms in its normal direction, $\hat{\mathbf{n}}^U$ or $\hat{\mathbf{n}}^L$ depending on inequality, upon contact with the end effector. By calculating the maximum deflection $n = n^{max}$ based on a force limit, we convert \mathcal{N} into \mathcal{P} , the end effector poses $\mathbf{r}(q)$ that apply less than maximum force. Our approach also adds an additional hyperplane per vertex during the set expansion, between \mathbf{c}_i^i to \mathbf{c}_i^{i+1} , to conservatively bound the environment’s force when two hyperplanes are deflected.

elastic modulus are generally sufficient for assumptions (4)-(5). Assumption (6) has been demonstrated in prior work on tissue mechanics [52].

B. Construction of a Safe Contact Set

We now seek a calculation that produces a set \mathcal{P} of tip positions that map to \mathcal{F}^{safe} :

$$\mathcal{P} = \{\mathbf{r} | \|\mathbf{F}_i(\mathbf{r})\| \leq F^{max}, \forall i = 1 \dots P\}, \quad (1)$$

i.e., locations in space that the robot’s tip can enter while never exerting greater than F^{max} on any one surface, so $\mathcal{P} = \{\mathbf{r} | \mathbf{F}(\mathbf{r}) \in \mathcal{F}^{safe}\}$. We next demonstrate that such a set exists, is itself a convex polytope, and is easily calculated by linear operations on \mathbf{H} and \mathbf{h} .

1) *Preprocessing:* Our approach preprocesses a given \mathcal{N} to put its rows into standard slope-intercept form, simplifying our later calculations without loss of generality. Assuming some original \mathbf{H}_o and \mathbf{h}_o are given for \mathcal{N} ,

$$\mathbf{N} = \left(\text{diag} \left(\begin{bmatrix} \mathbf{H}_o & \begin{bmatrix} 0 \\ 1 \end{bmatrix} \end{bmatrix} \right) \right)^{-1}, \quad \mathbf{H} = \mathbf{N}\mathbf{H}_o, \quad \mathbf{h} = \mathbf{N}\mathbf{h}_o, \quad (2)$$

$$\therefore \mathbf{H}\mathbf{r} = \mathbf{h} \Rightarrow \begin{bmatrix} -m_1 & 1 \\ -m_2 & 1 \\ \vdots & \vdots \end{bmatrix} \mathbf{r} = \begin{bmatrix} h_1 \\ h_2 \\ \vdots \end{bmatrix} \quad (3)$$

Readers can interpret this calculation by noting how $\mathbf{H}_o[0 \ 1]^T$ pulls out the second column of \mathbf{H}_o , and therefore \mathbf{N} divides each row by this element.

Next, we organize \mathbf{H} and \mathbf{h} into two blocks depending on the direction of the inequality, recalling that a “bounded below” constraint of the form $\mathbf{H}_i\mathbf{r} \geq h_i$ is also $-\mathbf{H}_i\mathbf{r} \leq -h_i$. With this sign adjustment,

$$\mathbf{H} = \begin{bmatrix} \mathbf{H}_U \\ \mathbf{H}_L \end{bmatrix} = \begin{bmatrix} -m_1 & 1 \\ \vdots & \vdots \\ m_P & -1 \end{bmatrix}, \quad \mathbf{h} = \begin{bmatrix} \mathbf{h}_U \\ \mathbf{h}_L \end{bmatrix}.$$

This separation is relevant in the calculation of the unit vectors $\hat{\mathbf{n}}$ pointing in the direction opposite the inequality.

2) *A Polytope Representation of the Safe Contact Set:* Converting the implicit set representation of \mathcal{P} into an explicit representation is trivial given our assumptions.

Lemma 1: Force-Safe Kinematics Set. The set \mathcal{P} in eqn. (1) is equivalent to

$$\mathcal{P} = \{\mathbf{r} | \mathbf{H}'\mathbf{r} \leq \mathbf{h}'\} \quad (4)$$

where, per assumption (3), each \mathbf{H}'_i, h'_i represent the \mathcal{L}'_i with a deformation $n_i = n^{max}$, and where

$$n^{max} = \psi^{-1}(F^{max}).$$

Proof: First, $\|\mathbf{F}_i(n_i)\| = \|\psi(n_i)\hat{\mathbf{n}}_i\| = \psi(n_i)$, since $\psi > 0$ is nonnegative, per assumptions (4)-(5). Therefore, $\psi(n_i) \leq F^{max} \Rightarrow n_i \leq \psi^{-1}(F^{max})$ per assumptions (5)-(6). Setting $n^{max} = \psi^{-1}(F^{max})$, our safety inequality becomes $n_i \leq n^{max} \forall i$.

Then construct the plane \mathcal{L}'_i using $\mathbf{n}_i^{max} = n^{max}\hat{\mathbf{n}}_i$ by inverting the relationship in assumption (2), i.e., $\mathcal{L}_i = \{\mathbf{r} + \mathbf{n}_i^{max}, \forall \mathbf{r} \in \mathcal{L}\}$. Since this is a linear translation, \mathcal{L}'_i must be in the form of $\mathbf{H}'_i\mathbf{r} = h'_i$ as expected. Therefore,

$$\mathbf{H}'_i\mathbf{r} \leq h'_i \Rightarrow n(\mathbf{r})_i \leq n^{max} \Rightarrow \|\mathbf{F}_i\| \leq F^{max}.$$

Concatenate all \mathbf{H}'_i, h'_i as rows as \mathbf{H}', \mathbf{h}' to obtain the intersection $\mathbf{H}\mathbf{r} \leq \mathbf{r}$ where $\|\mathbf{F}_i\| \leq F^{max} \forall i$, which is \mathcal{P} in eqn. (4). ■

Remark 1: Lemma 1 is a mathematically formal way of stating our intuition: “translate each line in \mathcal{N} outwards by a distance n^{max} to obtain \mathcal{P} .”

3) *Calculating the Safe Contact Polytope:* Though we have proven that \mathbf{H}'_i and h'_i exist and are sufficient to as a kinematic description of a force-safe set, we must still calculate them. Here, we show that $\mathbf{H}' = \mathbf{H}$ and that $h'_i = h_i + z_i$, i.e., a scalar translation, which is intuitive: our half-planes do not change their slope.

Consider row i so that $\mathbf{H}_i = [-m_i \ 1]$. A short calculation reveals two unit vectors normal to the line $\mathbf{H}_i\mathbf{r} = h_i$,

$$\hat{\mathbf{n}}_i^U = \frac{1}{\sqrt{m_i^2 + 1}} \begin{bmatrix} -m_i \\ 1 \end{bmatrix}, \quad \hat{\mathbf{n}}_i^L = -\hat{\mathbf{n}}_i^U. \quad (5)$$

Here, $\hat{\mathbf{n}}^U$ points in the \mathbf{E}_2 direction, since $\hat{\mathbf{n}}^U \cdot \mathbf{E}_2 > 0$, and vice-versa for $\hat{\mathbf{n}}^L$. We propose these names since $\hat{\mathbf{n}}^U$ points away from the no-contact set for $\mathbf{H}^U, \mathbf{h}^U$, and vice versa for $\mathbf{H}^L, \mathbf{h}^L$, see Fig. 3. With some arithmetic on the set of all points on the line $\mathbf{H}_i\mathbf{r} = h_i$ as the nonhomogeneous solution $\mathbf{r} = s[1 \ m_i]^\top + [0 \ h_i]^\top + n^{max}\hat{\mathbf{n}}_i$, where s is an arbitrary parameter, the translated set corresponds to

$$[-m_i \ 1] \mathbf{r} = h_i + n^{max}\sqrt{m^2 + 1} \quad (6)$$

for both $\hat{\mathbf{n}}^U$ and $\hat{\mathbf{n}}^L$. Therefore, $h'_i = h_i + n^{max}\sqrt{m^2 + 1}$ and $\mathbf{H}'_i = \mathbf{H}_i$. Apply eqn. (6) for all rows i to obtain \mathbf{H}' and \mathbf{h}' , obtaining \mathcal{P} in eqn. (4).

C. A Correction at the Vertices

Readers might observe a nuance of trigonometry in the set \mathcal{P} . Though each half-plane’s individual safety condition holds, the set \mathcal{P} does contain regions where $\|\mathbf{r} - \text{proj}_{\mathcal{N}}\mathbf{r}\| > n^{max}$: the tip is too far away from the no-contact set. This occurs in particular when $\text{proj}_{\mathcal{N}}\mathbf{r}$ is one of the vertices in \mathcal{N} , where the distance from \mathcal{N} is then really a ball (circle) around the vertex, as two “forces” are applied, $\mathbf{F} = \mathbf{F}_i + \mathbf{F}_{i+1}$. In other words, the regions around the vertices of \mathcal{P} are in fact force-unsafe, as they are outside these circles, so the constraint $n_i \leq n^{max} \forall i$ is insufficient.

We propose a conservative under-approximation of the safe region that maintains convexity and linearity. Consider the region around the vertex \mathbf{c}_i between the i -th and $i+1$ -th half plane. Define the two vectors $\mathbf{c}_i^i = \mathbf{c}_i + \mathbf{n}_i$ and $\mathbf{c}_i^{i+1} = \mathbf{c}_i + \mathbf{n}_{i+1}$, referring to Fig. 3. Then, concatenate row $P+i+1$ to $\{\mathbf{H}', \mathbf{h}'\}$ with m and h as the slope/intercept of the line passing through these points, with a sign correction per upper/lower directionality of $\hat{\mathbf{n}}^U$ or $\hat{\mathbf{n}}^L$ for polytope faces $i, i+1$, details omitted for brevity. Then, some arithmetic gives that $n_{P+i+1} \leq n^{max}$, satisfying the conditions of Lemma 1 by eliminating the dashed regions in Fig. 3 from \mathcal{P} .

IV. KINEMATICS AND DYNAMICS MODEL

Having established an expression for a task-space set of poses that maps to the robot-environment force, we next seek a state to task space model. For this proof-of-concept, we propose piecewise constant curvature (PCC) kinematics of a soft robot manipulator paired with the augmented body model of Della Santina et al. [30]. This approach gives both $\mathbf{r}(\mathbf{q})$ with states $\mathbf{q} \in \mathbb{R}^N$ as well as $\dot{\mathbf{x}} = f(\mathbf{x}, \mathbf{u})$.

We briefly summarize here and defer to prior work for full details on these models [53], [30] and their applicability to planar soft robots in the absence of gravitational loads. Here, the robot is represented with one subtended angle q_i per CC segment of length L_i for $i = 1 \dots N$, see Fig. 2. PCC kinematics admit a transformation matrix $\mathbf{T}_i^{i+1}(\mathbf{q})$ from one CC segment to the next, giving the end effector position as $\mathbf{r}(\mathbf{q}) = (\sum_{i=0}^{N-1} \mathbf{T}_i^{i+1}(\mathbf{q}))\mathbf{r}_0$.

For the dynamics, the augmented body model represents one CC segment as a series of z -many translation and rotation joints, as a virtual rigid robot manipulator, states $\xi_i \in \mathbb{R}^z$. A user then selects a kinematic constraint $m_i(\cdot) : \mathbb{R} \mapsto \mathbb{R}^z$, where $m_i(q_i) = \xi_i$, aligning e.g. the center of mass of the PCC segment with that of the virtual augmented body. For this manuscript, we choose Della Santina et. al.’s proof of concept RPPR virtual augmented body, $m_i = [\frac{q_i}{2}, L_i \frac{\sin(q_i)/2}{q_i}, L_i \frac{\sin(q_i)/2}{q_i}, \frac{q_i}{2}]^\top$, with one mass between the prismatic joints. Some applications of the chain rule on the full N -segment state, $\xi = m(\mathbf{q})$, give $\dot{\xi} = \mathbf{J}_m(\mathbf{q})\dot{\mathbf{q}}$ and $\ddot{\xi} = \dot{\mathbf{J}}_m(\mathbf{q}, \dot{\mathbf{q}})\dot{\mathbf{q}} + \mathbf{J}_m(\mathbf{q})\ddot{\mathbf{q}}$. Inserting these Jacobians into the manipulator equation for ξ , assuming some elastic damping and spring forces at each joint, converts a Nz -dimensional ODE into our N -dimensional expression:

$$\mathbf{M}(\mathbf{q})\ddot{\mathbf{q}} + \mathbf{C}(\mathbf{q}, \dot{\mathbf{q}})\dot{\mathbf{q}} + \mathbf{D}\dot{\mathbf{q}} + \mathbf{K}\mathbf{q} = \mathbf{J}^\top f_{ext} \quad (7)$$

For the control input, past work [54] demonstrates an approximation of pneumatic actuation as external forces, $\mathbf{J}^\top f_{ext} = \boldsymbol{\tau}$, viewed as virtual torques on the body. And as in past work [30], [55], we calibrate these virtual torques using a least squares fit to pneumatic pressures $\mathbf{u} \in \mathbb{R}^N$. So, $\boldsymbol{\tau} = \Lambda \mathbf{u}$ with $\Lambda = \text{diag}([\lambda_1, \dots, \lambda_N])$ fit from data.

Minor rearranging gives the final equations of motion with states $\mathbf{x} = [\mathbf{q}^\top \dot{\mathbf{q}}^\top]^\top$ as $\dot{\mathbf{x}} = f(\mathbf{x}) + g(\mathbf{x})\mathbf{u}$, with:

$$f = \left[\mathbf{M}^{-1} (\mathbf{C}\dot{\mathbf{q}} + \mathbf{D}\dot{\mathbf{q}} + \mathbf{K}\mathbf{q}) \right], \quad g = \left[\begin{array}{c} 0 \\ \mathbf{M}^{-1}\Lambda \end{array} \right] \quad (8)$$

We emphasize that these dynamics are control-affine, satisfying a key criterion of our method below.

V. SAFETY-CRITICAL CONTROL OF SOFT ROBOT MANIPULATOR FORCES USING CONTROL BARRIER FUNCTIONS

Having established both a set of kinematic end-effector states corresponding to force safety, \mathcal{P} , as well as the control-affine dynamics of our robot with $f(\mathbf{x})$ and $g(\mathbf{x})$, we now synthesize a control system to render \mathcal{P} invariant under the dynamics.

A. Control Barrier Functions For Force Safety

Many techniques are possible to enforce invariance of a state constraint in a control-affine dynamical system, but the approach of *control barrier functions* (CBFs) has the significant benefit of real-time feedback, possible by formulating a quadratic program [14]. To apply CBFs to our problem, we follow Rauscher et al. [16] in defining a set of scalar constraints $b_i(\cdot) : \mathbb{R}^{2N} \mapsto \mathbb{R}$, such that the set of safe states \mathcal{C} is defined as superlevel sets of these constraints, $\mathcal{C} = \{\mathbf{x} \mid b_i(\mathbf{x}) > 0 \forall i\}$. For our problem statement, these are the rows of the polytope \mathcal{P} with the forward kinematics inserted,

$$b_i(\mathbf{r}(\mathbf{q})) = h'_i - \mathbf{H}'_i \mathbf{r}(\mathbf{q}), \quad i = 1 \dots P \quad (9)$$

Next, we must define a control barrier function $B_i(\mathbf{x})$ per constraint, each of which must be the inverse of a class- κ function and be such that $\mathcal{L}_g B_i(\mathbf{x}) \neq 0$, where \mathcal{L} is the Lie derivative. We refer to prior work for more detailed justifications [16] (Defn. 3-4). Considering our soft robot manipulator with dynamics of the form in eqn. (7)-(8), our constraint function $b_i(\mathbf{r}(\mathbf{q}))$ has a relative degree two since \dot{b}_i depends on the system's control input \mathbf{u} . Consequently, we adopt the barrier function from [16], [56],

$$B_i(\mathbf{x}) = -\ln \left(\frac{b_i(\mathbf{x})}{1 + b_i(\mathbf{x})} \right) + a_E \frac{b_E \dot{b}_i(\mathbf{x})^2}{1 + b_E \dot{b}_i(\mathbf{x})^2} \quad (10)$$

where $b_i(\mathbf{x})$ and $\dot{b}_i(\mathbf{x})$ are the constraint function and its derivative respectively while a_E and b_E are tuning constants. Prior work has shown that eqn. (10) is a valid CBF for relative degree two systems. We note that small values of a_E , $b_E > 0$ result in more conservative behavior of the soft robot manipulator's end effector, while larger values reduce this

conservativeness, allowing for less restrictive motion near the safety constraint.

Using this barrier function, we can write a constraint that, if satisfied by a control input \mathbf{u} , ensures that the system states \mathbf{x} remain within the \mathcal{C} set (per [20], [16], [14], [22]),

$$L_f B_i(\mathbf{x}) + L_g B_i(\mathbf{x}) \mathbf{u} - \frac{\gamma_i}{B_i(\mathbf{x})} \leq 0 \quad \forall i \quad (11)$$

where $\gamma_i > 0$ is an additional tuning constant that indicates the rate of growth of the barrier function (higher γ is less conservative). Using the f and g from the dynamics in eqn. (8), these Lie derivatives become:

$$\mathcal{L}_f B = \mathbf{J}_B f = \mathbf{J}_B \dot{\mathbf{x}}, \quad \mathcal{L}_g B = \mathbf{J}_B g = \frac{\partial B}{\partial \mathbf{q}} \mathbf{M}^{-1} \Lambda \quad (12)$$

where \mathbf{J}_B is the Jacobian of the barrier function (10), taking advantage of the robot's kinematics,

$$\mathbf{J}_B = \frac{\partial B_i}{\partial \mathbf{x}} = \frac{\partial B}{\partial \mathbf{r}} \cdot \frac{\partial \mathbf{r}}{\partial \mathbf{x}} = \left[\begin{array}{cc} \frac{\partial B}{\partial \mathbf{q}} & \frac{\partial B}{\partial \dot{\mathbf{q}}} \end{array} \right] \quad (13)$$

which can be calculated e.g. using MATLAB's symbolic toolbox.

B. Feedback Controller with Control Barrier Functions

Our goal then becomes calculation of a feedback control law $\mathbf{u}(\mathbf{x})$ that satisfies eqn. (11) while also attempting to perform some nominal task. Here, we assume that there is an existing (unsafe) nominal controller, $\mathbf{u}_{nom}(\mathbf{x})$, for example the computed torque law from [54]. Following the literature [16], we adopt a quadratic program (QP) that minimizes the squared norm of the error between this nominal signal and the applied signal, $\|\mathbf{u} - \mathbf{u}_{nom}\|^2 = \mathbf{u}^\top \mathbf{u} - 2\mathbf{u}^\top \mathbf{u}_{nom} + \mathbf{u}_{nom}^\top \mathbf{u}_{nom}$. Dropping the constant term and inserting eqn. (11) as a constraint, our calculation becomes a QP:

$$\begin{aligned} \mathbf{u}^*(\mathbf{x}) = \arg \min_{\mathbf{u}} \quad & \mathbf{u}^\top \mathbf{u} - 2\mathbf{u}^\top \mathbf{u}_{nom} \\ \text{s. t.} \quad & \mathbf{A}(\mathbf{x}) \mathbf{u} \leq \mathbf{b}(\mathbf{x}) \end{aligned} \quad (14)$$

where \mathbf{u} is our decision variable since \mathbf{x} is held constant at each timestep, and

$$\mathbf{A}(\mathbf{x}) = \begin{bmatrix} \mathcal{L}_{g_1} B_1 & \dots & \mathcal{L}_{g_m} B_1 \\ \vdots & & \vdots \\ \mathcal{L}_{g_1} B_P & \dots & \mathcal{L}_{g_m} B_P \end{bmatrix}, \quad \mathbf{b}(\mathbf{x}) = \begin{bmatrix} \frac{\gamma_1}{B_1} - \mathcal{L}_f B_1 \\ \vdots \\ \frac{\gamma_P}{B_P} - \mathcal{L}_f B_P \end{bmatrix} \quad (15)$$

This controller satisfies the following safety condition:

Theorem 1: Force Safety Under CBF-Based QP Feedback. If a soft robot governed by PCC kinematics and the dynamics of eqn. (7)-(8) starts at $\mathbf{q}(0) \in \mathcal{C}$ defined by eqn. (9), applying the control law $\mathbf{u}(\mathbf{x}(t)) = \mathbf{u}^*(\mathbf{x}(t))$ by solving eqn. (14) renders the set \mathcal{P} from eqn. (4) invariant, i.e., $\mathbf{F}(t) \in \mathcal{F}^{safe} \forall t > 0$.

Proof: From Theorem 1 of Rauscher et al. [16], the control law of eqn. (14) and barrier function (10) will ensure that $b_i(\mathbf{x}(t)) > 0 \forall t$. We have defined \mathcal{C} as this set, now

invariant. Correspondingly, $\mathbf{x} \in \mathcal{C} \Rightarrow \mathbf{r} \in \mathcal{P}$. By Lemma 1, $\mathbf{r}(t) \in \mathcal{P} \forall t$ meets Definition 1. ■

Remark 2: Readers are referred to prior work for details such as Lipschitz continuity conditions, admissibility, set intersections of multiple constraints, etc., as Theorem 1 does not introduce any novel theoretical considerations.

VI. SIMULATION VALIDATION

Our approach was validated in a dynamics simulation of eqn. (7)-(8). Results show that Theorem 1 holds.

A. Simulation Setup and Calibration

The simulation from [55] was used for this validation task, now calibrated against a physical prototype of a two-segment planar soft robot actuated by antagonistic pneumatic pressure inputs (Fig. 2). Each segment has length 0.122 m and mass 0.13 kg. Here, the robot is fully actuated, by mapping negative control inputs to opposing pneumatic chambers p_j, p_{j+1} . We calibrate the constants in the \mathbf{K}, \mathbf{D} and Λ matrices of the dynamics model using a least squares fit of data points obtained from the hardware prototype's open-loop motion using motor babbling, as suggested by [54]. The simulation uses forward Euler numerical integration with $\Delta_t = 1e^{-5}$ sec, with a control frequency of 1000 Hz.

B. Nominal Controller

As proof-of-concept, we employ an open-loop sequence of sinusoids for $\mathbf{u}_{nom}(t)$, mimicking random motions in a sensitive environment: $u_{nom,j} = A_j \sin(2\pi\omega_j t)$. We tune the amplitudes and frequencies to achieve desired coverage of the task space. With the robot's pressure inputs measured in hecto-Pascals, $A_j = 45$ hPa and $\omega_j = 0.0167$ Hz will reach bending angles of approximately $q_i = \pm 25^\circ$, a large workspace.

C. Safe Controller Tests

We implemented eqn. (14) in MATLAB's `quadprog` with these dynamics. The environment was taken as one constraint for clarity of exposition, with $\mathbf{H}_1 = [0.36, 1.0]$, $h_1 = 0.15$, and $F^{max} = 0.2232$. The deformation was modeled as a linear spring, $\psi(n) = kn$, with a spring constant of $k = 11.16$. These arbitrary values correspond to visual identification of the robot's motion in hardware, contact with an environment approximately halfway through its sinusoid, with an anticipated maximum displacement of the environment of $n^{max} \approx 4.5$ cm.

We executed the controller with four sets of tuning constants for the $B_1(\mathbf{x})$ CBF, shown in Table I, corresponding to conservativeness (None, Low, Medium, High), chosen by hand. The 'None' condition removes the CBF constraint, so $\mathbf{u}^* = \mathbf{u}_{nom}$.

For each simulation, we postprocess to calculate the end effector position $\mathbf{r} = [r_x, r_y]^T$, as well as the simulated force and simulated *safety margin*. We define the safety margin of the closed-loop trajectory in simulation as a normalized distance to the boundary of our safe set \mathcal{P} , i.e., $\rho(t) =$

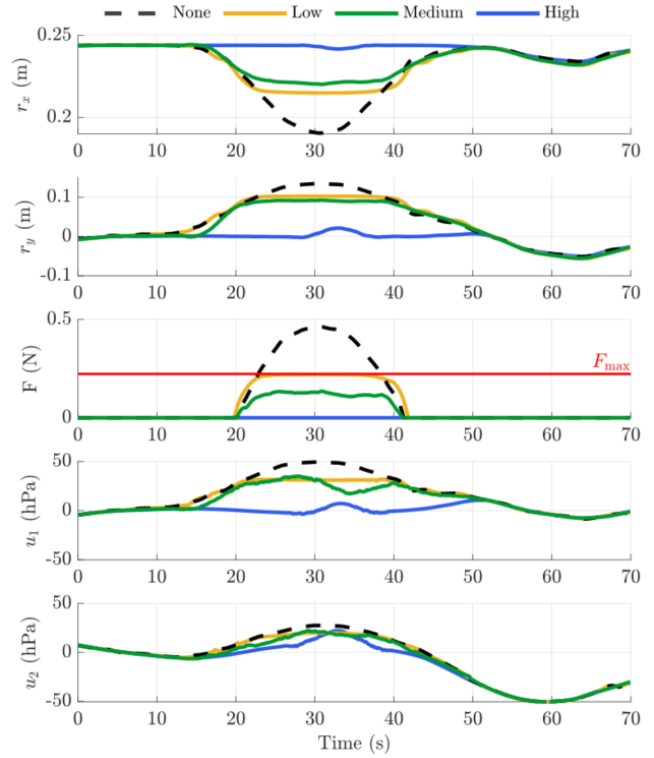


Fig. 4. Simulation results with three levels of conservativeness of CBF tuning constants all show that the robot's end effector is prevented from moving out of the unsafe set, when the unsafe \mathbf{u}_{nom} control (black dashed line) would violate safety.

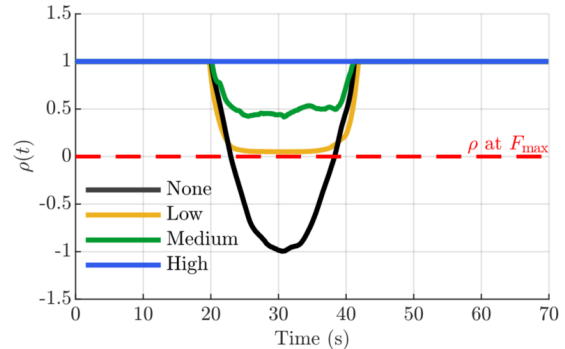


Fig. 5. All simulations with CBF-based control show a positive safety margin on force application. The most conservative CBF tuning (blue) prevents all environmental contact.

$(F^{max} - F(t))/F^{max} = (n^{max} - n(t))/n^{max}$, since the simulation has a one-to-one mapping between force and displacement. A safety margin of $\rho = 1$ indicates that the robot is not contacting the environment, and $\rho < 0$ indicates constraint violation. To calculate $F(t)$ and $\rho(t)$, we calculate $n(\mathbf{r}(t))$ for our one-environment surface, then invert the force-displacement relationship.

D. Simulation Results

Theorem 1 holds in all our tested simulations (Fig. 4), as a positive safety margin holds, $\rho(t) > 0$, Fig. 5. Without our CBF controller in the loop ('None,' black line), the robot violates the safe force constraint, third panel of Fig.

4, and reaches a negative safety margin ρ_{min} of -0.9955 . As we introduce the CBF controller at different levels of conservativeness (Low and Medium cases), the safety margin increases and stays above the critical threshold $\rho = 0$, which is the safety margin ρ at maximum force F_{max} as seen in Table I. At a high level of conservativeness, the safety margin remains constant at $\rho = 1$, indicating that the robot avoids contact with the environment entirely.

TABLE I
SAFETY MARGIN COMPARISON FOR DIFFERENT LEVELS OF
CONSERVATIVENESS

Conservativeness	$\mathbf{a_E}$	$\mathbf{b_E}$	γ	$hw \rho_{min}$	$sim \rho_{min}$
High	0.2	0.2	0.2	0.9956	1.0
Medium	2.0	2.0	2.0	0.1658	0.4162
Low	20.0	20.0	20.0	0.0916	0.0504
None	0.0	0.0	0.0	-0.2070	-0.9955

VII. HARDWARE EXPERIMENTS

We then tested the CBF-based controller in a hardware experiment corresponding to the simulation. As with the simulation validation, Theorem 1 held in all cases.

A. Hardware Platform

The soft limb used to calibrate the simulation was also used for a real-time control test (Fig. 6). The limb was placed in the environment with fiducial markers (AprilTags [57]) located at the start of the limb and at the end of every section, captured with an overhead camera and processed using OpenCV, with the bending angles \mathbf{q} calculated from the tag locations. The electronics and software infrastructure were based on prior work [19]. The chambers' pressure was controlled by a microcontroller with a low-level PID loop between a DC pump and proportional valve (iQ Volta), recorded by a pressure sensor (Honeywell MPRLS). Lastly, a flexible sheet of ABS was attached to a force gauge for use as the deformable surface. Its spring constant was calibrated using masses placed at the tip under gravitational loading, then it was placed in the environment aligned vertically with the robot's tip.

To calibrate the location of the force plate that matched the simulation setup, it was first approximately aligned in the plane by measurements from the origin. Then, a constant input was applied to the robot, $\mathbf{u} = \mathbf{u}_{TOUCH}$, where \mathbf{u}_{TOUCH} was taken from the simulation at the first point when the robot's end effector exits the no-contact set \mathcal{N} (i.e. the first time the robot touches its environment). The force plate was then adjusted manually while the robot was pressurized until the force readings became (almost) zero. In this way, the robot would contact its environment with the same input-to-kinematics mapping in hardware.

VIII. HARDWARE EXPERIMENTAL RESULTS

We then repeated the same tests as in simulation. This setup used a ROS2 MATLAB node to receive bending angles from OpenCV and send the outputs of quadprog to the

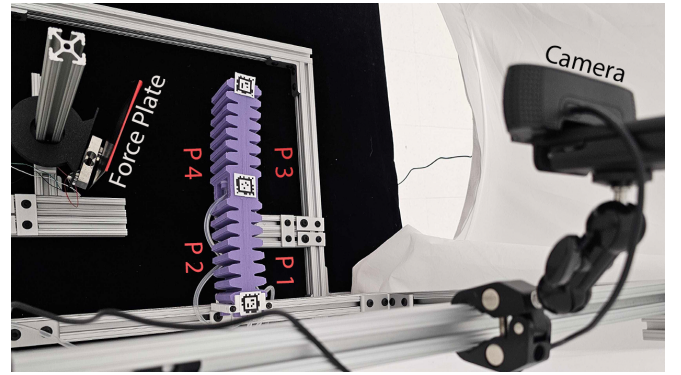


Fig. 6. Testing and limb set up for hardware validation of CBF-based control framework. In order to capture the states, \mathbf{q} , of our system, a camera was placed above the limb to record position data of three Apriltags placed along the limb. Control inputs from the CBF are fed into the low level controller to increase/decrease the measured pressures (P_1, P_2, P_3, P_4) in the limb. The force plate was first calibrated to match the position in simulation and force measurements are used to demonstrate that force safety was achieved.

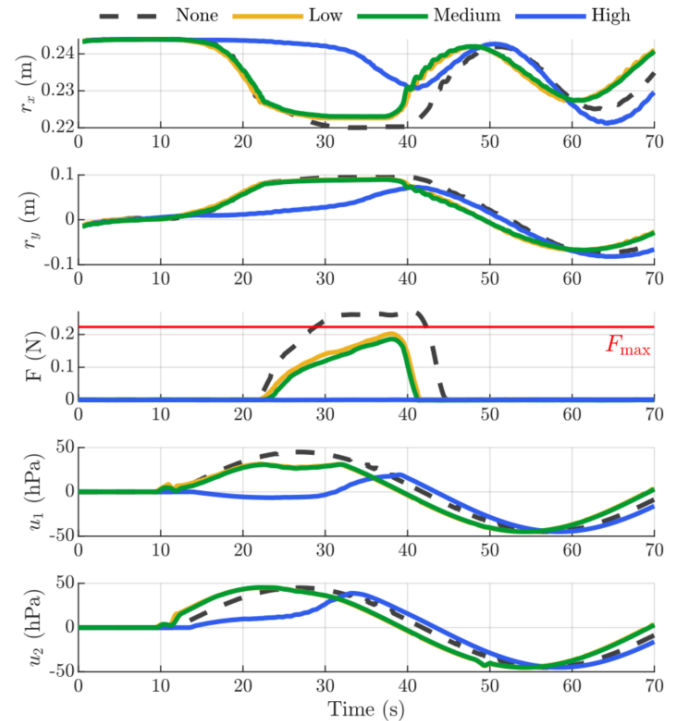


Fig. 7. Measured position r_x and r_y in meters, force F in Newtons, and controller inputs u_1 and u_2 in hPa for four levels of conservativeness in the CBFs: None, Low, Medium, High. Results show that the inclusion of CBFs guarantees the limb never exceeds F_{max} .

microcontroller. As with simulation, each of the three CBF conservativeness levels (Table I) produces a positive safety margin (Fig. 7, 8). As expected, decreasing conservativeness leads to a smaller worst-case safety margin ρ_{min} , as the robot's tip is allowed closer to the unsafe set boundary. The 'High' conservative tuning does not make contact with the flexible force plate. The 'Medium' and 'Low' conservative tunings make contact, but maintain their forces below the limit. Without the CBF ('None'), the force constraint is violated. The control input traces (panels 4 and 5 in Fig. 7) show that the CBF controller reshapes the nominal pressure waveforms primarily during the critical contact period (approximately

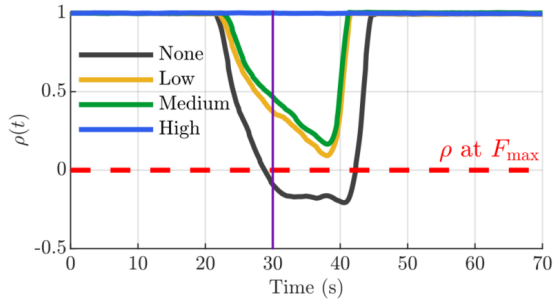


Fig. 8. Safety margin $\rho(t)$ for the hardware experiments. The red, dashed line, outlines the minimum allowed ρ value to guarantee force safety. The purple thin line at $t = 30s$ allows for quick comparison of the ρ value for the superimposed cases in Fig. 10.

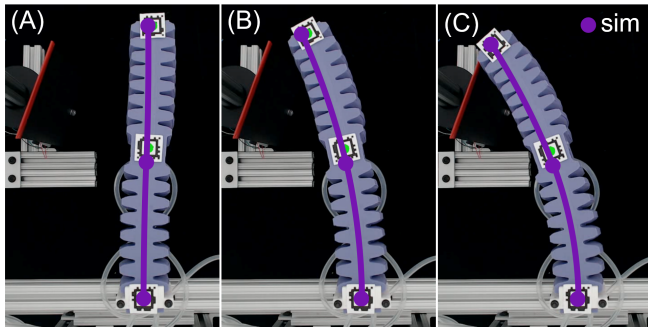


Fig. 9. Comparison of the simulation’s kinematics versus hardware at three key points during a corresponding test demonstrates the alignment between the model and experiment.

20 to 40 sec), preserving the shape of the input elsewhere, just as seen in our simulation results.

A. Visualizations: Simulation vs. Hardware, Environment Deformation

To provide a clear visual comparison of the simulation results, Fig. 9 overlays the simulation’s output at three key points versus the hardware test, demonstrating that the kinematics align well qualitatively. Similarly, Fig. 10 overlays two hardware tests: the robot’s configuration at the 30 sec timestep for the ‘None’ and ‘Medium’ cases (indicated by the purple vertical line in Fig 8). The difference in force plate deflection was visually apparent, corresponding to the disparity in force and safety margin values at that time. The ‘Medium’ case exhibits a relatively more conservative deflection, limiting the contact force exerted on the force plate and resulting in a safer, lower-impact interaction.

IX. DISCUSSION

This article proposes the use of control barrier functions to guarantee force safety in soft robot manipulators when placed into deformable environments with a known maximum safe force. Results in both simulation and hardware experiments on a pneumatic soft robot confirm that the proposed safety-critical control approach successfully satisfies an invariance condition on the force applied by a soft robot end-effector. The close correspondence between hardware and simulation results reinforces both the effectiveness and the fidelity of our proposed control framework. At all levels of tuning

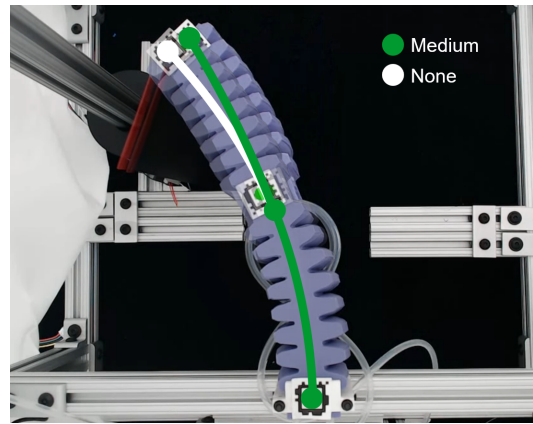


Fig. 10. Image of case None, labeled in white, superimposed onto case Medium, labeled in green, at $t = 30s$ to show the difference in position reached between the two cases.

the controller’s constants for conservativeness, the trends in minimum safety margin ρ_{\min} , end-effector position r_x , r_y , force profiles $F(t)$, force plate deflection n and control inputs u_1 , u_2 remain consistent across both simulation and hardware. With our method, the F_{\max} can be chosen prior to setting the barrier functions to tune the level of safety needed for the chosen task and environment.

Although our results are consistent in terms of safety margin, multiple sources of error exist that cause the trajectories between simulation vs. hardware to be qualitatively different. Comparing Fig. 4 against Fig. 7, the same input sequence of pressures causes a different sequence of tip positions. The ‘Low’ versus ‘Medium’ tunings produce different trajectories in simulation but qualitatively the same trajectory in hardware. Our setup’s assumptions include the PCC dynamics and no gravity, but also a high bandwidth pressure input (whereas our hardware has a finite response time), fast sensing of positions and velocities (whereas our computer vision has a slow frame rate and a finite difference for \dot{q}), normal displacement of the environment (whereas the hardware has a 3D motion), environmental properties (linear stiffness) and all other typical hardware difficulties (camera distortion, unmodeled disturbances, etc). Future efforts will investigate each of these sources of error.

In addition, the hardware unsafe motion shows a blocking behavior at 30-40 sec, when the robot is pushed up against the flexible force plate, whereas the simulation has free motion. This behavior arises from our dynamics model: for this proof-of-concept, we do not model the dynamics of the environment on the robot’s tip, and rely on the assumption that the environment is more compliant than the robot in low-force regimes. The hardware test shows that this assumption did not hold in practice in more extreme unsafe circumstances, but was a realistic approximation for safe regions with low contact.

Consequently, the conclusions from this work are limited to this specific proof-of-concept, though the method may be generalized and re-tested in relaxed conditions. For example, only one environmental surface was tested, with the environment known exactly.

Lastly, many nuances of tuning were observed in our tests. Very large values of a_E, b_E, γ could violate the constraint in both simulation and hardware, which we attribute primarily to discretization time: the robot moves too fast within a short period of time and exits the safe set before the next control calculation. Oscillations were also commonly observed, as were large input magnitudes with very conservative CBFs (very small a_E, b_E, γ , approx. 10x less than Table I).

X. CONCLUSION AND FUTURE WORK

This work represents, to the authors' knowledge, the first formal closed-loop safety-verified controller for a soft robot manipulator's environmental interactions. The work here suggests an entirely different perspective on control of soft robots, one which simultaneously avoids the paradoxical issues of precision and tracking control in a soft system, while also giving an engineering analysis to claims of 'safety' in soft robotics. Extending and applying this concept may provide the intelligence needed to bring soft manipulation into the real-world environments envisioned as their eventual application.

To do so, future work will extend this concept in many ways in addition to addressing sources of error. In some tests, the robot's tip was observed to be force-safe, but other portions of the robot's body would contact the force plate. Since the CBF used in this article only takes into consideration the position of the end-effector, this method would fail in guaranteeing force safety and encourages a method of taking into consideration the pose of the whole body. Future work will therefore consider ensuring invariance of all points along the robot's backbone into the set \mathcal{C} . Similarly, it is possible that higher-performance barrier function candidates may be chosen (e.g., High Order CBFs [20]) which allow the robot to move faster in more complex environments. The environments may be relaxed to nonconvex sets, those that vary in time or are probabilistic, sequences of conditions on forces and states, velocity constraints, grasping conditions, or an enormous number of other formal methods considerations. It is the authors' hope that this direction in autonomy and intelligence proves widely fruitful for the soft robotics community.

REFERENCES

- [1] A. Albu-Schaffer, M. Fischer, G. Schreiber, F. Schoeppe, and G. Hirzinger, "Soft robotics: what cartesian stiffness can obtain with passively compliant, uncoupled joints?," in *2004 IEEE/RSJ International Conference on Intelligent Robots and Systems (IROS) (IEEE Cat. No.04CH37566)*, vol. 4, pp. 3295–3301 vol.4, 2004.
- [2] D. Trivedi, A. Lotfi, and C. D. Rahn, "Geometrically exact models for soft robotic manipulators," *IEEE Transactions on Robotics*, vol. 24, no. 4, pp. 773–780, 2008.
- [3] M. Cianchetti, M. Calisti, L. Margheri, M. Kuba, and C. Laschi, "Bioinspired locomotion and grasping in water: the soft eight-arm octopus robot," *Bioinspiration & biomimetics*, vol. 10, no. 3, p. 035003, 2015.
- [4] S. Sanan, M. H. Ornstein, and C. G. Atkeson, "Physical human interaction for an inflatable manipulator," in *2011 Annual International Conference of the IEEE Engineering in Medicine and Biology Society*, pp. 7401–7404, 2011.
- [5] C. Majidi, "Soft robotics: A perspective—current trends and prospects for the future," *Soft Robotics*, vol. 1, no. 1, pp. 5–11, 2014.
- [6] H. Abidi and M. Cianchetti, "On intrinsic safety of soft robots," *Frontiers in Robotics and AI*, vol. 4, 2017.
- [7] N. Enayati, E. De Momi, and G. Ferrigno, "Haptics in robot-assisted surgery: Challenges and benefits," *IEEE Reviews in Biomedical Engineering*, vol. 9, pp. 49–65, 2016.
- [8] M. Vasic and A. Billard, "Safety issues in human-robot interactions," in *2013 IEEE International Conference on Robotics and Automation*, pp. 197–204, May 2013.
- [9] P. A. Lasota, T. Fong, and J. A. Shah, "A Survey of Methods for Safe Human-Robot Interaction," *Foundations and Trends in Robotics*, vol. 5, pp. 261–349, May 2017.
- [10] T. Dang and O. Maler, "Reachability analysis via face lifting," in *Hybrid Systems: Computation and Control* (T. A. Henzinger and S. Sastry, eds.), Lecture Notes in Computer Science, (Berlin, Heidelberg), pp. 96–109, Springer, 1998.
- [11] A. K. Akametalu, J. F. Fisac, J. H. Gillula, S. Kaynama, M. N. Zeilinger, and C. J. Tomlin, "Reachability-based safe learning with Gaussian processes," in *53rd IEEE Conference on Decision and Control*, pp. 1424–1431, Dec. 2014. ISSN: 0191-2216.
- [12] J. F. Fisac, A. K. Akametalu, M. N. Zeilinger, S. Kaynama, J. Gillula, and C. J. Tomlin, "A General Safety Framework for Learning-Based Control in Uncertain Robotic Systems," *IEEE Transactions on Automatic Control*, vol. 64, pp. 2737–2752, July 2019. Conference Name: IEEE Transactions on Automatic Control.
- [13] C. Massera Filho, M. H. Terra, and D. F. Wolf, "Safe Optimization of Highway Traffic With Robust Model Predictive Control-Based Cooperative Adaptive Cruise Control," *IEEE Transactions on Intelligent Transportation Systems*, vol. 18, pp. 3193–3203, Nov. 2017.
- [14] A. D. Ames, J. W. Grizzle, and P. Tabuada, "Control barrier function based quadratic programs with application to adaptive cruise control," in *53rd IEEE Conference on Decision and Control*, pp. 6271–6278, 2014.
- [15] R. Funada, M. Santos, J. Yamauchi, T. Hatanaka, M. Fujita, and M. Egerstedt, "Visual Coverage Control for Teams of Quadcopters via Control Barrier Functions," in *2019 International Conference on Robotics and Automation (ICRA)*, pp. 3010–3016, May 2019. ISSN: 2577-087X.
- [16] M. Rauscher, M. Kimmel, and S. Hirche, "Constrained robot control using control barrier functions," in *2016 IEEE/RSJ International Conference on Intelligent Robots and Systems (IROS)*, pp. 279–285, Oct. 2016. ISSN: 2153-0866.
- [17] C. T. Landi, F. Ferraguti, S. Costi, M. Bonfè, and C. Secchi, "Safety Barrier Functions for Human-Robot Interaction with Industrial Manipulators," in *2019 18th European Control Conference (ECC)*, pp. 2565–2570, June 2019.
- [18] A. P. Sabelhaus, Z. J. Patterson, A. T. Wertz, and C. Majidi, "Safe supervisory control of soft robot actuators," *Soft Robotics*, vol. 11, no. 4, pp. 561–572, 2024. PMID: 38324015.
- [19] M. L. Anderson, R. Jing, J. C. Pacheco Garcia, I. Yang, S. Alizadeh-Shabdiz, C. DeLorey, and A. P. Sabelhaus, "Maximizing Consistent High-Force Output for Shape Memory Alloy Artificial Muscles in Soft Robots," in *IEEE International Conference on Soft Robotics (RoboSoft)*, Apr. 2024.
- [20] Z. J. Patterson, W. Xiao, E. Sologuren, and D. Rus, "Safe control for soft-rigid robots with self-contact using control barrier functions," in *2024 IEEE 7th International Conference on Soft Robotics (RoboSoft)*, pp. 151–156, IEEE, 2024.
- [21] K. P. Tee, S. S. Ge, and E. H. Tay, "Barrier lyapunov functions for the control of output-constrained nonlinear systems," *Automatica*, vol. 45, no. 4, pp. 918–927, 2009.
- [22] A. D. Ames, S. Coogan, M. Egerstedt, G. Notomista, K. Sreenath, and P. Tabuada, "Control barrier functions: Theory and applications," in *2019 18th European Control Conference (ECC)*, pp. 3420–3431, 2019.
- [23] Y. Chen, A. Singletary, and A. D. Ames, "Guaranteed obstacle avoidance for multi-robot operations with limited actuation: A control barrier function approach," *IEEE Control Systems Letters*, vol. 5, no. 1, pp. 127–132, 2021.
- [24] H.-S. Chang, U. Halder, E. Gribova, A. Tekinalp, N. Naughton, M. Gazzola, and P. G. Mehta, "Controlling a CyberOctopus Soft Arm with Muscle-like Actuation," in *2021 60th IEEE Conference on Decision and Control (CDC)*, pp. 1383–1390, Dec. 2021. ISSN: 2576-2370.
- [25] H. Li, L. Xun, G. Zheng, and F. Renda, "Discrete Cosserat Static Model-Based Control of Soft Manipulator," *IEEE Robotics and Automation Letters*, pp. 1–8, 2023. Conference Name: IEEE Robotics and Automation Letters.
- [26] A. Doroudchi, Z. Qiao, W. Zhang, and S. Berman, "Implementation of a Cosserat Rod-Based Configuration Tracking Controller on a Multi-Segment Soft Robotic Arm," in *2023 IEEE/RSJ International*

- Conference on Intelligent Robots and Systems (IROS)*, pp. 620–626, Oct. 2023. ISSN: 2153-0866.
- [27] C. Della Santina, C. Duriez, and D. Rus, “Model-Based Control of Soft Robots: A Survey of the State of the Art and Open Challenges,” *IEEE Control Systems Magazine*, vol. 43, pp. 30–65, June 2023. Conference Name: IEEE Control Systems Magazine.
- [28] A. Bajo and N. Simaan, “Hybrid motion/force control of multi-backbone continuum robots,” *The International Journal of Robotics Research*, vol. 35, pp. 422–434, Apr. 2016. Publisher: SAGE Publications Ltd STM.
- [29] M. Hachen, C. Shentu, S. Lilge, and J. Burgner-Kahrs, “A Non-Linear Model Predictive Task-Space Controller Satisfying Shape Constraints for Tendon-Driven Continuum Robots,” *IEEE Robotics and Automation Letters*, vol. 10, pp. 2438–2445, Mar. 2025.
- [30] C. Della Santina, M. Bianchi, G. Grioli, F. Angelini, M. Catalano, M. Garabini, and A. Bicchi, “Controlling Soft Robots: Balancing Feedback and Feedforward Elements,” *IEEE Robotics Automation Magazine*, vol. 24, pp. 75–83, Sept. 2017.
- [31] Z. J. Patterson, A. P. Sabelhaus, and C. Majidi, “Robust Control of a Multi-Axis Shape Memory Alloy-Driven Soft Manipulator,” *IEEE Robotics and Automation Letters*, vol. 7, Apr. 2022.
- [32] F. J. Abu-Dakka and M. Saveriano, “Variable impedance control and learning—a review,” *Frontiers in Robotics and AI*, vol. 7, 2020.
- [33] M. Dyck, A. Sachtler, J. Klodmann, and A. Albu-Schäffer, “Impedance Control on Arbitrary Surfaces for Ultrasound Scanning Using Discrete Differential Geometry,” *IEEE Robotics and Automation Letters*, vol. 7, pp. 7738–7746, July 2022. Conference Name: IEEE Robotics and Automation Letters.
- [34] D. Bruder, X. Fu, R. B. Gillespie, C. D. Remy, and R. Vasudevan, “Data-Driven Control of Soft Robots Using Koopman Operator Theory,” *IEEE Transactions on Robotics*, pp. 1–14, 2020. Conference Name: IEEE Transactions on Robotics.
- [35] D. A. Haggerty, M. J. Banks, E. Kamenar, A. B. Cao, P. C. Curtis, I. Mezić, and E. W. Hawkes, “Control of soft robots with inertial dynamics,” *Science Robotics*, vol. 8, p. eadd6864, Aug. 2023. Publisher: American Association for the Advancement of Science.
- [36] D. Braganza, D. M. Dawson, I. D. Walker, and N. Nath, “A neural network controller for continuum robots,” *IEEE Transactions on Robotics*, vol. 23, no. 6, pp. 1270–1277, 2007.
- [37] T. G. Thuruethel, E. Falotico, F. Renda, and C. Laschi, “Model-based reinforcement learning for closed-loop dynamic control of soft robotic manipulators,” *IEEE Transactions on Robotics*, vol. 35, no. 1, pp. 124–134, 2019.
- [38] A. Pereira and C. Thomas, “Challenges of machine learning applied to safety-critical cyber-physical systems,” *Machine Learning and Knowledge Extraction*, vol. 2, pp. 579–602, 11 2020.
- [39] J. Wang and A. Chortos, “Control strategies for soft robot systems,” *Advanced Intelligent Systems*, vol. 4, no. 5, p. 2100165, 2022.
- [40] P. Schegg and C. Duriez, “Review on generic methods for mechanical modeling, simulation and control of soft robots,” *PLOS ONE*, vol. 17, p. e0251059, Jan. 2022. Publisher: Public Library of Science.
- [41] M. Thieffry, A. Kruszewski, C. Duriez, and T.-M. Guerra, “Control Design for Soft Robots Based on Reduced-Order Model,” *IEEE Robotics and Automation Letters*, vol. 4, pp. 25–32, Jan. 2019.
- [42] E. Ménager, A. Bilger, W. Jallet, J. Carpentier, and C. Duriez, “Condensed Semi-Implicit Dynamics for Trajectory Optimization in Soft Robotics,” in *2024 IEEE 7th International Conference on Soft Robotics (RoboSoft)*, pp. 808–815, Apr. 2024. ISSN: 2769-4534.
- [43] L. Brunke, M. Greeff, A. W. Hall, Z. Yuan, S. Zhou, J. Panerati, and A. P. Schoellig, “Safe Learning in Robotics: From Learning-Based Control to Safe Reinforcement Learning,” *Annual Review of Control, Robotics, and Autonomous Systems*, vol. 5, no. 1, pp. 411–444, 2022. eprint: <https://doi.org/10.1146/annurev-control-042920-020211>.
- [44] N. Kochdumper, H. Krasowski, X. Wang, S. Bak, and M. Althoff, “Provably Safe Reinforcement Learning via Action Projection Using Reachability Analysis and Polynomial Zonotopes,” *IEEE Open Journal of Control Systems*, vol. 2, pp. 79–92, 2023.
- [45] X. Li, Z. Serlin, G. Yang, and C. Belta, “A formal methods approach to interpretable reinforcement learning for robotic planning,” *Science Robotics*, vol. 4, p. eaay6276, Dec. 2019. Publisher: American Association for the Advancement of Science.
- [46] R. Sepulchre, “Safety-Critical Control Systems [About this Issue],” *IEEE Control Systems Magazine*, vol. 43, pp. 5–6, Apr. 2023. Conference Name: IEEE Control Systems Magazine.
- [47] R. Sepulchre, “Robust Performance? Resilient Safety! [From the Editor],” *IEEE Control Systems Magazine*, vol. 43, pp. 3–4, June 2023. Conference Name: IEEE Control Systems Magazine.
- [48] L. Balasubramanian, T. Wray, and D. D. Damian, “Fault tolerant control in shape-changing internal robots,” in *2020 IEEE International Conference on Robotics and Automation (ICRA)*, pp. 5502–5508, 2020.
- [49] Y. Feng, T. Ide, H. Nabae, G. Endo, R. Sakurai, S. Ohno, and K. Suzumori, “Safety-enhanced control strategy of a power soft robot driven by hydraulic artificial muscles,” *Robomech Journal*, vol. 8, pp. 1–16, 2021.
- [50] M. Stölzle and C. D. Santina, “Input-to-State Stable Coupled Oscillator Networks for Closed-form Model-based Control in Latent Space,” in *Neural Information Processing Systems (NeurIPS)*, 2024.
- [51] S. B. Liu and M. Althoff, “Online Verification of Impact-Force-Limiting Control for Physical Human-Robot Interaction,” in *2021 IEEE/RSJ International Conference on Intelligent Robots and Systems (IROS)*, pp. 777–783, Sept. 2021. ISSN: 2153-0866.
- [52] T. Fujikawa, R. Sugiura, R. Nishikata, and T. Nishimoto, “Critical contact pressure and transferred energy for soft tissue injury by blunt impact in human-robot interaction,” in *2017 17th International Conference on Control, Automation and Systems (ICCAS)*, pp. 867–872, Oct. 2017.
- [53] R. J. Webster and B. a. Jones, “Design and Kinematic Modeling of Constant Curvature Continuum Robots: A Review,” *The International Journal of Robotics Research*, vol. 29, pp. 1661–1683, Nov. 2010.
- [54] C. Della Santina, R. K. Katzschmann, A. Bicchi, and D. Rus, “Model-based dynamic feedback control of a planar soft robot: trajectory tracking and interaction with the environment,” *The International Journal of Robotics Research*, vol. 39, no. 4, pp. 490–513, 2020.
- [55] A. Dickson, J. C. P. Garcia, R. Jing, M. L. Anderson, and A. P. Sabelhaus, “Real-Time Trajectory Generation for Soft Robot Manipulators Using Differential Flatness,” in *IEEE International Conference on Soft Robotics (RoboSoft)*, Apr. 2025. arXiv:2412.08568 [cs].
- [56] S.-C. Hsu, X. Xu, and A. D. Ames, “Control barrier function based quadratic programs with application to bipedal robotic walking,” in *2015 American Control Conference (ACC)*, pp. 4542–4548, 2015.
- [57] J. Wang and E. Olson, “AprilTag 2: Efficient and robust fiducial detection,” in *2016 IEEE/RSJ International Conference on Intelligent Robots and Systems (IROS)*, pp. 4193–4198, Oct. 2016. ISSN: 2153-0866.